Nanoscale Advances

ROYAL SOCIETY OF CHEMISTRY

COMMUNICATION

View Article Online
View Journal | View Issue

Cite this: *Nanoscale Adv.*, 2022, **4**, 4035

Received 29th July 2022
Accepted 23rd August 2022

DOI: 10.1039/d2na00498d

rsc.li/nanoscale-advances

One-pot synthesis of robust dendritic sulfur quantum dots for two-photon fluorescence imaging and "off–on" detection of hydroxyl radicals and ascorbic acid†

Jisuan Tan,[a] Yiheng Song,[a] Xuanjun Dai,[a] Guan Wang[b] and Li Zhou *[a]

The straightforward preparation of fluorescent sulfur quantum dots (SQDs) with good photostability and biocompatibility and multifunction remains a challenge. Herein, a simple method to improve the performance of SQDs is reported, that is, using hyperbranched polyglycerol (HPG) as a ligand to direct the synthesis of dendritic HPG-SQD nanocomposites from cheap elemental sulfur. Thanks to the protection of HPG, the HPG-SQDs show much better biocompatibility and photostability as compared with the widely reported polyethylene glycol (PEG) ligand-capped SQDs (PEG-SQDs). In addition, the HPG-SQDs also present excellent aqueous solubility, stable fluorescence against environmental variation, good cell uptake capability, and strong single- and two-photon fluorescence. Moreover, the HPG-SQDs display sensitive and selective fluorescence "off–on" behavior to hydroxyl radicals (˙OH) and ascorbic acid (AA), respectively, and thereby hold potential as a fluorescent switch to detect ˙OH and AA. For the first time, the utilization of two-photon fluorescence of HPG-SQDs to monitor ˙OH and AA in cells is demonstrated in this study.

Introduction

Sulfur quantum dots (QDs), novel metal-free luminescent nanodots, have attracted more and more attention because of their unique composition and attractive attributes, as well as numerous potential applications.[1] Additionally, SQDs can now be directly synthesized from cheap elemental sulfur.[2–5] However, most of the surface ligands reported so far cannot completely stabilize SQDs, resulting in poor photostability of SQDs and difficulty of tolerating long time UV-light illumination, which seriously limits the practical applications of SQDs.[4,6,7] For instance, the fluorescence intensity of polyethylene glycol (PEG)-capped SQDs declined by 48% after exposure to a UV lamp for 10 min.[4] In addition, although SQDs do not contain heavy metal ions, they are generally slightly more toxic than other metal-free fluorescent nanodots, such as carbon dots and graphene quantum dots.[8,9] Therefore, there is still an urgent need to explore an effective strategy to produce SQDs with high photostability and good biocompatibility.

As one of the most crucial reactive oxygen species *in vivo*, hydroxyl radicals (˙OH) can cause oxidative damage to various biomolecules including proteins, nucleic acids, carbohydrates and lipids, and thus their production process and content are related to various diseases (*e.g.*, tumors, cardiovascular diseases, and aging).[10] Ascorbic acid (AA), also known as vitamin C, has good antioxidant effects and is an essential nutrient for the treatment and prevention of a variety of diseases. Nevertheless, an excessive intake or lack of AA may lead to diarrhea, acidosis, cancer and kidney stones.[11] So far, a variety of sensing technologies have been developed for the detection of ˙OH and AA, among which fluorescence detection technology has attracted much attention due to its high sensitivity, simple operation and low cost.[12] Nevertheless, most reported fluorescent probes suffer from the disadvantages of high toxicity, low sensitivity, poor water solubility and high cost. As such, the development of an applicable fluorescent probe for sensitive detection of ˙OH and AA remains a challenge. On the other hand, although SQDs have been studied as a fluorescent probe for bioimaging,[13] the reported SQDs generally present short wavelength emission (*e.g.*, blue fluorescence) and are excited using UV light, which is prone to photobleaching and is susceptible to the organism's own fluorescence. In this regard, two-photon fluorescence imaging technology can effectively overcome the above drawbacks due to its advantages of low spontaneous fluorescence, large penetration depth and less

[a]*Key Laboratory of New Processing Technology for Nonferrous Metal and Materials (Ministry of Education), Guangxi Key Laboratory of Optical and Electronic Materials and Devices, and College of Materials Science and Engineering, Guilin University of Technology, Guilin 541004, China. E-mail: zhouli@glut.edu.cn*

[b]*Institute of Sustainability for Chemicals, Energy and Environment, A*STAR, Singapore, 138634, Singapore*

† Electronic supplementary information (ESI) available. See https://doi.org/10.1039/d2na00498d

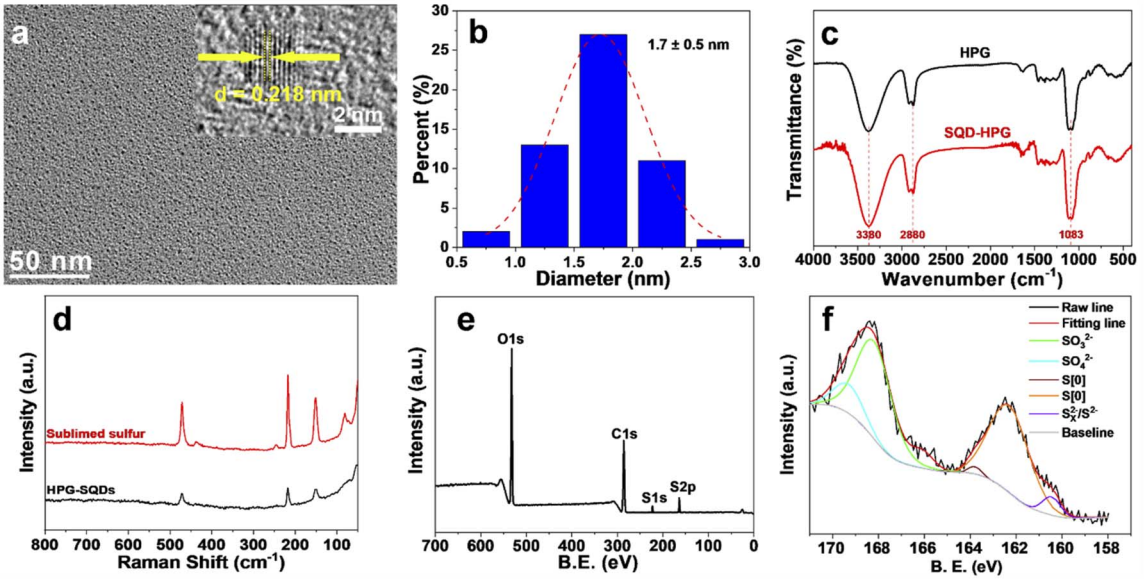

Fig. 1 (a) Representative TEM and HRTEM (inset) images of HPG-SQDs. (b) Size-distribution histograms of HPG-SQDs. (c) FTIR spectra of HPG and HPG-SQDs. (d) Raman spectra of sublimed sulfur and HPG-SQDs. XPS survey (e) and S 2p (f) spectra of HPG-SQDs.

photobleaching.[14] However, to date, the employment of SQDs as a two-photon fluorescence probe has rarely been studied.

In this contribution, we report a simple one-pot strategy to prepare multifunctional dendritic SQDs from cheap elemental sulfur by employing hyperbranched polyglycerol (HPG) as a ligand (Fig. 1a). Different from previously reported ligands, the biocompatible HGP with a highly branched molecular structure and numerous hydroxyl groups can simultaneously endow SQDs with superior photostability and good biocompatibility.[15] Moreover, the obtained HPG-SQDs can be utilized not only as a single-photon fluorescence switch for sensing of ˙OH and AA in water, but also as a two-photon fluorescence probe for imaging and monitoring of ˙OH and AA in cells.

Results and discussion

The synthesis process of the HPG-SQDs is depicted in Scheme 1. Fluorescent HPG-SQDs can be easily prepared by agitating an aqueous mixture of sublimed sulfur, NaOH, and HPG in an oxygen atmosphere at 95 °C for 24 h. The formation of HPG-SQDs could be achieved by the following reactions.[4,16]

$$\text{Elemental sulfur} + \text{NaOH} \rightarrow \text{Na}_2\text{S} + \text{Na}_2\text{SO}_3 + \text{H}_2\text{O} \quad (1)$$

$$(x-1)\text{S} + \text{S}^{2-} \rightarrow \text{S}_x^{2-} \quad (2)$$

$$\text{S}_x^{2-} + \text{O}_2 + \text{HPG} \rightarrow \text{HPG-SQDs} + \text{SO}_3^{2-} + \text{SO}_4^{2-} \quad (3)$$

Firstly, the elemental sulfur can react with NaOH to produce sodium polysulfide (Na_2S_x). Subsequently, the pure oxygen atmosphere can accelerate the oxidation of polysulfide ions (S_x^{2-}) to zero-valent sulfur atoms and facilitate the production of SQDs in the presence of HPG.[4]

Notably, no fluorescent product was formed without addition of sublimed sulfur or HPG. After purification by dialysis against deionized water, a transparent aqueous solution of HPG-SQDs was obtained and it could emit bright cyan fluorescence under a 365 nm UV lamp (Scheme 1 and Fig. S1†).

Transmission electron microscopy (TEM) images (Fig. 1a) show that HPG-SQDs have a small and uniform size, with a mean diameter of about 1.7 nm (Fig. 1b). The corresponding high-resolution TEM (HRTEM) image (Fig. 1a) indicates that HPG-SQDs possess obvious lattice fringes with a crystal plane spacing of 0.218 nm, which is similar to other reported SQDs.[4,17,18] The Fourier transformed infrared spectroscopy (FTIR) results (Fig. 1c) reveal that all absorption peaks of HPG-SQDs are consistent with those of HPG. Hence, no new chemical bonds were formed between HPG and SQDs. Furthermore, the Raman spectrum of HPG-SQDs (Fig. 1d) is very similar to that of sublimed sulfur, which demonstrated that the resultant fluorescent nanodots are SQDs. The X-ray photoelectron spectroscopy (XPS) result (Fig. 1e) shows that the HPG-SQDs sample consists of carbon, oxygen, and sulfur elements. The corresponding high-resolution XPS S 2p spectrum (Fig. 1f) indicates

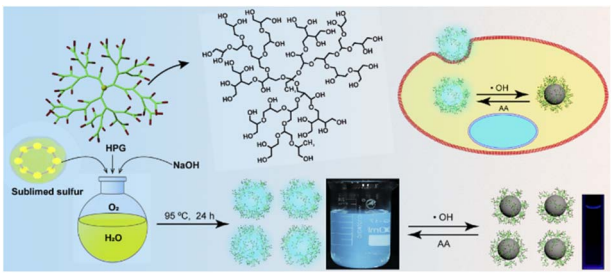

Scheme 1 Schematic illustration of the synthesis of HPG-SQDs for fluorescence "off–on" sensing of ˙OH and AA.

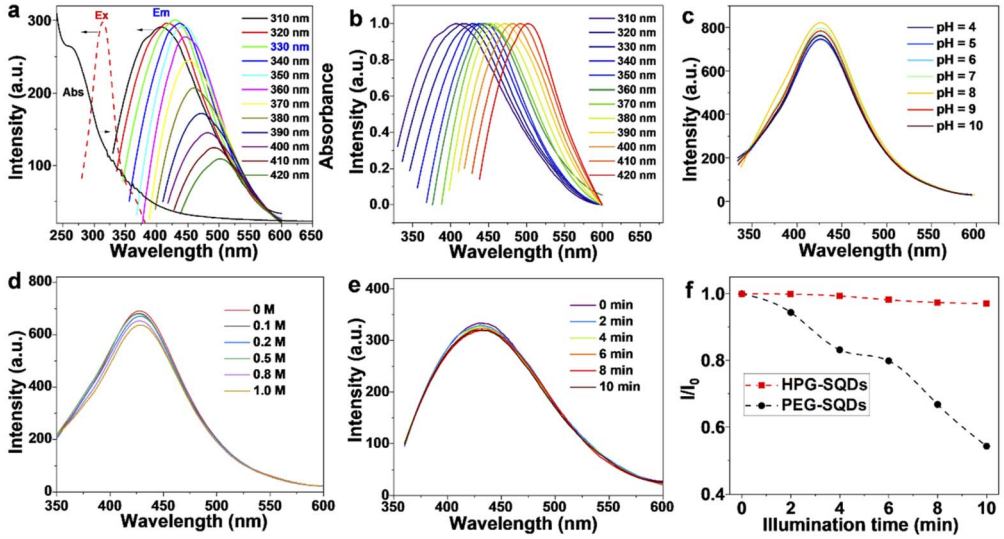

Fig. 2 (a) UV-vis absorption (Abs), excitation (Ex) and emission (Em) spectra of HPG-SQDs. (b) Normalized emission spectra of HPG-SQDs with various λ_{ex}. Effects of pH (c), NaCl concentration (d), and UV light illumination (e) on the fluorescence intensity of HPG-SQDs. (f) Relative fluorescence intensity (I_0/I) of HPG-SQDs and PEG-SQDs after illumination with 365 nm UV light for different times. I_0 and I represent the fluorescence intensity of SQDs before and after illumination of UV light for different time, respectively.

the presence of four kinds of sulfur including atomic sulfur (S [0]), SO_3^{2-}, SO_4^{2-} and S_x^{2-}/S^{2-} in HPG-SQDs,[1e,2,4] which is consistent with the reaction equations. The sulfur content in HPG-SQDs was determined by elemental analysis (EA). The EA result (Table S1†) showed that the mass fractions of sulfur, carbon, hydrogen and oxygen were 32.48 wt%, 30.37 wt%, 6.23 wt% and 30.92 wt% (calculated result), respectively.

Owing to the capping of HPG, the HPG-SQDs present superior aqueous solubility and stability, and there was no precipitate in its aqueous solution even after being stored for 3 months. In the UV-vis absorption spectrum of HPG-SQDs (Fig. 2a), an absorption peak at about 264 nm can be observed, which is attributed to the n → π* transition of sulfur atoms.[16,17] Like other reported SQDs,[4,18,19] the emission peaks of HPG-SQDs can be tuned to some extent by manipulating the excitation wavelength (λ_{ex}) (Fig. 2a and b). With the λ_{ex} of 330 nm, the strongest emission peak appeared at around 427 nm (Fig. 2a), which agrees well with the excitation spectrum. Meanwhile, the absolute fluorescence quantum yield (QY) of HPG-SQDs was measured to be 6.8%, which compares favorably to that of many reported SQDs.[1] The fluorescence decay curve of HPG-SQDs (Fig. S2†) can be fitted by a triple-exponential function as follows:

$$Y(t) = A_1 \exp(-t/\tau_1) + A_2 \exp(-t/\tau_2) + A_3 \exp(-t/\tau_3) \quad (4)$$

where A_1, A_2 and A_3 represent the fractional contributions of time-resolved decay lifetimes of τ_1, τ_2 and τ_3, respectively.

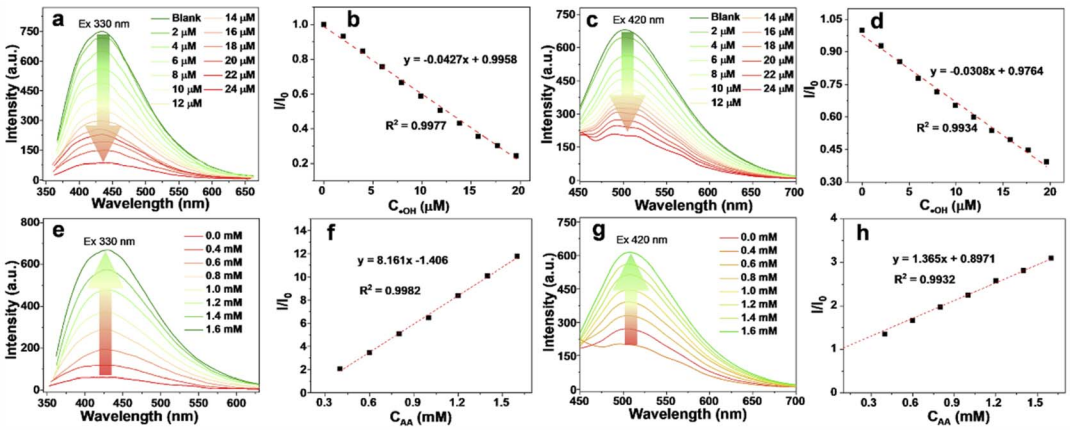

Fig. 3 Emission spectra (a and c) and the corresponding I/I_0 values (b and d) of HPG-SQDs upon adding various concentrations of •OH with excitation wavelengths of 330 nm (a and b) and 420 nm (c and d), respectively. Emission spectra (e and g) and the corresponding I/I_0 values (f and h) of the mixture of HPG-SQDs (100 μg mL^{-1}) and •OH (24 μM) before and after adding AA solution with excitation wavelengths of 330 nm (e and f) and 420 nm (g and h), respectively.

Considering the relatively low QY of HPG-SQDs, the dynamic photophysical behavior of HPG-SQDs mainly obeys the non-radiation path rather than the radiation path.[20] The average lifetime of the HPG-SQDs was calculated to be 2.35 ns, similar to other reported SQDs.[7,11] In addition, the HPG-SQDs presented stable fluorescence against long time storage (Fig. S3†) and environmental variation, such as pH changing in the range of 4–10 (Fig. 2c) or mixing with a high concentration of NaCl (*e.g.* 1.0 M) (Fig. 2d), indicating that the HPG-SQDs hold potential to be utilized in complex environments. Remarkably, the HPG-SQDs also exhibited much higher photostability than widely reported polyethylene glycol (PEG)-capped SQDs (PEG-SQDs). After illuminating the HPG-SQDs with 365 nm UV light for 10 min, no obvious fluorescence decline was observed (Fig. 2e). In contrast, the fluorescence intensity of PEG-SQDs declined by 48% (Fig. 2f). This is because the HPG macromolecule possesses a large number of hydroxyl groups and a highly branched macromolecular structure, which can endow the SQDs with good photo-oxidation resistance.

Interestingly, the HPG-SQDs display remarkable fluorescence quenching behavior towards ˙OH. As shown in Fig. 3a and c, regardless of λ_{ex} at 330 nm or 420 nm, the fluorescence intensity of HPG-SQDs declined continuously with increasing concentration of ˙OH. After mixing with 20 μM of ˙OH, the fluorescence intensity of HPG-SQDs decreased by 76.2% and 60.6% with a λ_{ex} of 330 nm or 420 nm, respectively. Additionally, this fluorescence quenching process could reach equilibrium within 2 min (Fig. S4†). All these results indicate that the ˙OH can quench the fluorescence of HPG-SQDs. Furthermore, the quenching efficiency (I/I_0, where I and I_0 represent the fluorescence intensity of HPG-SQDs in the presence and absence of ˙OH, respectively) was highly dependent on the concentration of ˙OH with a good linear correlation in the range of 0.5–20 μM, offering an opportunity for the quantitative detection of ˙OH (Fig. 3b and d). The limit of detection at the excitation wavelength of 330 nm (signal-to-noise is 3) was calculated to be 0.23 ± 0.03 μM, which is superior to those of numerous reported nanoprobes (see Table S2†).[10a,12] To probe the quenching mechanism, the UV-vis absorption spectra and fluorescence–decay curves of HPG-SQDs before and after mixing ˙OH were compared. Clearly, the addition of ˙OH leads to the red shift of the absorption peak (from 264 nm to 290 nm) (Fig. S5†) and the shortening of fluorescence lifetime (from 2.35 ns to 2.06 ns) (Fig. S2†). Therefore, the fluorescence quenching process may be a dynamic process. The oxidation of the surface of HPG-SQDs by ˙OH would affect the non-radiative path of HPG-SQDs.

In addition to high sensitivity, the HPG-SQDs also showed excellent selectivity. In comparison with ˙OH, the fluorescence quenching effect of other common metal ions (*e.g.*, Fe^{2+}, Fe^{3+}, Ni^{2+}, K^{+}, Zn^{2+}, Mn^{2+}, Cu^{2+}, Mg^{2+}, Ag^{+}, Cd^{2+} and Pd^{2+}) (Fig. S6†) and molecules (*e.g.*, H_2O_2, AA, histidine, glycine, arginine, cysteine, glucose and lysine) (Fig. S7†) on HPG-SQDs was negligible or very slight even when their concentration was as high as 50 μM. It is worth noting that the quenched fluorescence can be effectively and selectively recovered by adding AA (Fig. S8†). No matter λ_{ex} was 330 nm (Fig. 3e) or 420 nm (Fig. 3g), the fluorescence intensity of the HPG-SQDs/˙OH system enhanced with increasing the addition amount of AA and presented a good linear relationship between 0.4 mM and 1.6 mM (Fig. 3f and h). In addition, the fluorescence recovery process can be completed within 3 min (Fig. S9†). It is noteworthy that the fluorescence lifetime of the HPG-SQDs/˙OH system recovered from 2.06 ns to 2.23 ns after AA addition (Fig. S2†), and meanwhile the absorption peak shifted from 290 nm to 264 nm (Fig. S5†), which was consistent with HPG-SQDs. Hence, this fluorescence recovery phenomenon induced by AA may be attributed to the fact that AA is a typical reducing agent, which can eliminate the oxidation effect of ˙OH to HPG-SQDs. Moreover, this fluorescence quenching/recovery behavior of HPG-SQDs is repeatable although the extent of switching back and forth gradually weakened (Fig. S10†). Therefore, the HPG-SQDs hold potential as a fluorescent nanoprobe for the sensitive detection of ˙OH and AA.

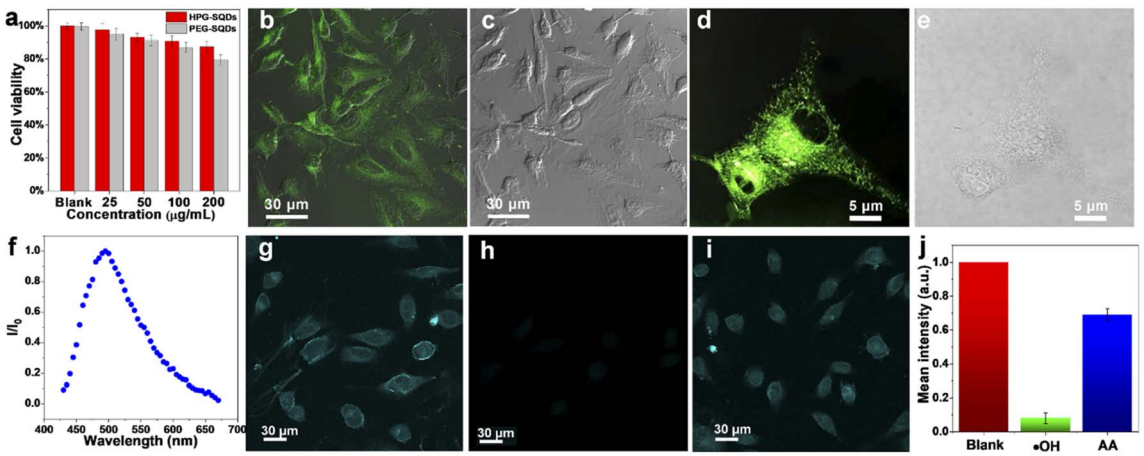

Fig. 4 (a) Cell viabilities of HeLa cells after incubation with HPG-SQDs and PEG-SQDs for 24 h, respectively. CLSM fluorescence (b and d) and bright field (c and e) images of HPG-SQDs (50 μg mL^{-1}) stained HeLa cells (λ_{ex} = 488 nm). (f) Two-photon fluorescence spectrum of HPG-SQDs with λ_{ex} of 800 nm. Two-photon fluorescence images of HeLa cells after incubation with HPG-SQDs, (g) followed by ˙OH (30 μM) (h) and AA (1.5 mM) (i), and the corresponding mean two-photon fluorescence intensity (j).

The toxicity of HPG-SQDs was evaluated with HeLa cells using thiazolyl blue tetrazolium bromide (MTT) assay. As shown in Fig. 4a, even after incubation with a high concentration of HPG-SQDs (*e.g.*, 100 μg mL^{-1}) for 24 h, the HeLa cells still displayed over 90% of cell viability. Moreover, the HPG-SQDs exhibited much lower cytotoxicity than that of widely reported PEG-SQDs with the same concentration, suggesting that the biocompatible HPG can endow the SQDs with good biocompatibility. In addition, utilizing fluorescent HPG-SQDs to stain HeLa cells was also investigated. Confocal laser-scanning microscopy (CLSM) images (Fig. 4b–e) show that the cell cytoplasm of HeLa cells could emit obvious green fluorescence after staining with HPG-SQDs (50 μg mL^{-1}), demonstrating the successful uptake of HPG-SQDs by the cells. However, in practical bioimaging applications, single-photon short-wavelength fluorescence imaging is susceptible to photobleaching and spontaneous fluorescence of organisms. Considering that two-photon fluorescence imaging technology can effectively overcome the above shortcomings, the two-photon fluorescence characteristics of HPG-SQDs were studied. Fortunately, the HPG-SQDs showed distinct two-photon fluorescence with an emission peak at about 495 nm under the excitation of an 800 nm femtosecond pulse laser (Fig. 4f). As such, using HPG-SQDs in two-photon fluorescence imaging and *in vitro* detection of $^{\bullet}OH$ and AA was further studied using a multiphoton fluorescence microscope (Fig. 4g–j and S11†). As depicted in Fig. 4g, the HeLa cells after incubation with HPG-SQDs (50 μg mL^{-1}) present bright two-photon fluorescence. In accordance with the single-photon emission spectra, the two-photon fluorescence of HeLa cells also weakened after addition of $^{\bullet}OH$ (Fig. 4h), and then recovered to a large extent after mixing in AA (Fig. 4i). The corresponding statistical analysis results showed that the two-photon fluorescence intensity of HPG-SQD stained HeLa cells decreased by nearly 90% after mixing in $^{\bullet}OH$ (30 μM), and then recovered to 70% after adding AA (1.5 mM) (Fig. 4j). To our knowledge, this is the first example of two-photon fluorescence detection in cells based on SQDs to date.

Conclusions

In conclusion, this study reports the first example of effective enhancement of photostability, biocompatibility and versatility of SQDs using a hyperbranched polymer ligand. Thanks to the introduction of multihydroxy biocompatible HPG, the dendritic HPG-SQD nanocomposites simultaneously showed superior aqueous solubility, stable fluorescence, good photostability, low cytotoxicity, good cell uptake capability, and strong single- and two-photon fluorescence. In addition, HPG-SQDs also exhibited sensitive and selective fluorescence quenching/recovery behavior to $^{\bullet}OH$ and AA, respectively, and thus could be employed as a fluorescent switch to detect $^{\bullet}OH$ and AA. Moreover, this study also demonstrated for the first time that the two-photon fluorescence of HPG-SQDs can be exploited to perform cell imaging and monitoring of $^{\bullet}OH$ and AA in cells.

Conflicts of interest

There are no conflicts to declare.

Acknowledgements

This work was supported by the National Natural Science Foundation of China (No. U21A2097), Natural Science Foundation of Guangxi Province (No. 2017GXNSFFA198002), and Bagui Scholar Program of Guangxi Province.

Notes and references

1 (*a*) P. Gao, G. Wang and L. Zhou, *ChemPhotoChem*, 2020, **4**, 5235–5244; (*b*) Y. Shi, P. Zhang, D. Yang and Z. Wang, *Chem. Commun.*, 2020, **56**, 10982–10988; (*c*) A. Pal, F. Arshad and M. P. Sk, *Adv. Colloid Interface Sci.*, 2020, **285**, 102274; (*d*) L. Liu, Y. Zhang, R. Yuan and H. Wang, *Anal. Chem.*, 2020, **92**, 15112–15119; (*e*) S. Li, D. Chen, F. Zheng, H. Zhou, S. Jiang and Y. Wu, *Adv. Funct. Mater.*, 2014, **24**, 7133–7138.

2 L. Shen, H. Wang, S. Liu, Z. Bai, S. Zhang, X. Zhang and C. Zhang, *J. Am. Chem. Soc.*, 2018, **140**, 7878–7884.

3 H. Wang, Z. Wang, Y. Xiong, S. Kershaw, T. Li, Y. Wang, Y. Zhai and A. Rogach, *Angew. Chem., Int. Ed.*, 2019, **58**, 7040–7044.

4 Y. Song, J. Tan, G. Wang, P. Gao, J. Lei and L. Zhou, *Chem. Sci.*, 2020, **11**, 772–777.

5 P. Gao, Z. Huang, J. Tan, G. Lv and L. Zhou, *ACS Sustainable Chem. Eng.*, 2022, **10**, 4634–4641.

6 Z. Huang, J. Lei, H. Ruan, Y. Gong, G. Wang and L. Zhou, *Microchem. J.*, 2021, **164**, 106031.

7 S. Rong, Q. Chen, G. Xu, F. Wei, J. Yang, D. Ren, X. Cheng, X. Xia, J. Li, M. Gao, Q. Hu and Y. Cen, *Sens. Actuators, B*, 2022, **353**, 131146.

8 (*a*) S. T. Yang, L. Cao, P. G. Luo, F. Lu, X. Wang, H. Wang, M. J. Meziani, Y. Liu, G. Qi and Y. P. Sun, *J. Am. Chem. Soc.*, 2009, **131**, 11308–11309; (*b*) S. Bayda, E. Amadio, S. Cailotto, Y. Frión-Herrera, A. Perosa and F. Rizzolio, *Nanoscale Adv.*, 2021, **3**, 5183–5221; (*c*) S. Zeng, J. Long, J. Sun, G. Wang and L. Zhou, *Carbohydr. Polym.*, 2022, **279**, 119015.

9 (*a*) Q. Liu, B. Guo, Z. Rao, B. Zhang and J. R. Gong, *Nano Lett.*, 2013, **13**, 2436–2441; (*b*) Y. Chong, Y. Ma, H. Shen, X. Tu, X. Zhou, J. Xu, J. Dai, S. Fan and Z. Zhang, *Biomaterials*, 2014, **35**, 5041–5048.

10 (*a*) S. Liu, J. Zhao, K. Zhang, L. Yang, M. Sun, H. Yu, Y. Yan, Y. Zhang, L. Wu and S. Wang, *Analyst*, 2016, **141**, 2296–2302; (*b*) Z. Li, T. Liang, S. Lv, Q. Zhuang and Z. Liu, *J. Am. Chem. Soc.*, 2015, **137**, 11179–11185.

11 (*a*) X. Lv, H. Man, L. Dong, J. Huang and X. Wang, *Food Chem.*, 2020, **326**, 126935; (*b*) Y. Duan, J. Tan, Z. Huang, Q. Deng, S. Liu, G. Wang, L. Li and L. Zhou, *Carbohydr. Polym.*, 2020, **249**, 116882; (*c*) Z. Wei, W. Lu, C. Pan, J. Ni, H. Zhao, G. Huang and C. Wang, *Dalton Trans.*, 2022, **51**, 10290–10297.

12 (*a*) Q. Zhao, R. Zhang, D. Ye, S. Zhang, H. Chen and J. Kong, *ACS Appl. Mater. Interfaces*, 2017, **9**, 2052–2058; (*b*) Y. Sun, L. Pang, X. Guo and H. Wang, *Microchim. Acta*, 2022, **189**, 60; (*c*) F. Shi, Y. Zhang, W. Na, X. Zhang, Y. Li and X. Su, *J. Mater. Chem. B*, 2016, **4**, 3278–3285.

13 (*a*) H. Ruan and L. Zhou, *Front. Bioeng. Biotechnol.*, 2022, **10**, 909727; (*b*) C. Zhang, P. Zhang, X. Ji, H. Wang, H. Kuang, W. Cao, M. Pan, Y. Shi and Z. Wang, *Chem. Commun.*, 2019, **55**, 13004–13007; (*c*) J. Lei, Z. Huang, P. Gao, J. Sun and L. Zhou, *Part. Part. Syst. Charact.*, 2021, **38**, 2000332; (*d*) F. Arshad, M. P. Sk, S. K. Maurya and H. R. Siddique, *ACS Appl. Nano Mater.*, 2021, **4**, 3339–3344.

14 (*a*) C. Yang, K. Chen, M. Chen, X. Hu, S. Y. Huan, L. Chen, G. Song and X. B. Zhang, *Anal. Chem.*, 2019, **91**(4), 2727–2733; (*b*) A. Zhu, Z. Luo, C. Ding, B. Li, S. Zhou, R. Wang and Y. Tian, *Analyst*, 2014, **139**, 1945–1952.

15 (*a*) D. Wilms, S. E. Stiriba and H. Frey, *Acc. Chem. Res.*, 2010, **43**, 129–141; (*b*) S. Abbina, S. Vappala, P. Kumar, E. M. Siren, C. C. La, U. Abbasi, D. E. Brooks and J. N. Kizhakkedathu, *J. Mater. Chem. B*, 2017, **5**, 9249–9277; (*c*) H. Frey and R. Haag, *Rev. Mol. Biotechnol.*, 2002, **90**, 257–267; (*d*) L. Zhou, J. Geng, G. Wang, J. Liu and B. Liu, *Polym. Chem.*, 2013, **4**, 5243–5251; (*e*) B. Huang, D. Wang, G. Wang, F. Zhang and L. Zhou, *J. Colloid Interface Sci.*, 2017, **508**, 214–221.

16 (*a*) S. Liu, H. Wang, A. Feng, J. Chang, C. Zhang, Y. E. Shi, Y. Zhai, V. Biju and Z. Wang, *Nanoscale Adv.*, 2021, **3**, 4271–4275; (*b*) Z. Huang, Y. Gao, Z. Huang, D. Chen, J. Sun and L. Zhou, *Microchem. J.*, 2021, **170**, 106656.

17 Y. Sheng, Z. Huang, Q. Zhong, H. Deng, M. Lai, Y. Yang, W. Chen, X. Xia and H. Peng, *Nanoscale*, 2021, **13**, 2519–2526.

18 G. Qiao, L. Liu, X. Hao, J. Zheng, W. Liu, J. Gao, C. Zhang and Q. Wang, *Chem. Eng. J.*, 2020, **382**, 122907.

19 L. Xiao, Q. Du, Y. Huang, L. Wang, S. Cheng, Z. Wang, T. N. Wong, E. K. L. Yeow and H. Sun, *ACS Appl. Nano Mater.*, 2019, **2**, 6622–6628.

20 F. Arshad and M. P. Sk, *ACS Appl. Nano Mater.*, 2020, **3**, 3044–3049.